An eight-year climatology of the warm-season severe thunderstorm environments over North China

Ruoyun Ma [a,b], Jianhua Sun [a,b,c,*], Xinlin Yang [d]

[a] Key Laboratory of Cloud-Precipitation Physics and Severe Storms, Institute of Atmospheric Physics, Chinese Academy of Sciences, Beijing 100029, China
[b] University of Chinese Academy of Sciences, Beijing 100049, China
[c] Southern Marine Science and Engineering Guangdong Laboratory (Zhuhai), Zhuhai 519000, China
[d] Key Laboratory of Regional Climate-Environment for Temperate East Asia, Institute of Atmospheric Physics, Chinese Academy of Sciences, Beijing, China

ABSTRACT

Using proximity soundings taken during the warm seasons (May–September) of 2011–2018 over North China, this work investigated the environments of severe thunderstorms that caused the following four types of convective hazards: only hail (H), only thunderstorm high winds (W), only short-duration heavy rainfall (R), and two or three types of the above three hazards (hybrid). The environments for non-severe thunderstorms and no-rain days were also studied for comparison. Soundings in each weather category were further classified into mountain and plain groups. A set of parameters was tested for skill in discriminating between various categories. Results indicate that the environments over the plains, compared with those over the mountains, are generally characterized by stronger instability, more moisture, and higher vertical wind shear. Over both mountains and plains, the precipitable water (PW) shows the greatest skill overall in discriminating between various categories; the instability parameters show considerable skill in discriminating between the severe thunderstorm, non-severe thunderstorm, and no-rain categories but rather limited skill in discriminating between the four severe thunderstorm categories; the wind shear parameters show very limited skill in discriminating between various categories; the lifting condensation level (LCL) distinguishes well the environments of no-rain and R from those of other categories; and the mid-tropospheric pseudo-equivalent potential temperature is the only parameter investigated here that shows utility in discriminating between H and W environments. Probability distributions in two-parameter spaces reveal that great variations exist regarding the environments under which different weather types are most likely to occur.

1. Introduction

Severe thunderstorms frequently cause short-duration heavy rainfall (SDHR), thunderstorm high winds (THWs), and hail over North China (Chen et al., 2013; Yang et al., 2017; Li et al., 2018b) and pose a great threat to life and property in this region. For example, the extreme rainfall event that occurred in Beijing on July 21, 2012 affected a flood-hit population of more than 160 million, caused 112 deaths in Hebei and Beijing, and incurred a direct economic loss in excess of RMB 10 billion (Sun et al., 2013). Forecasting severe thunderstorms over North China is particularly challenging, as storm activities are strongly influenced by the complex surface conditions, which feature high mountains, plains, and the Bohai sea from northwest to southeast, as well as large

metropolitan areas in the national capital Beijing (Sun and Yang, 2008; Chen et al., 2012; Chen et al., 2016a; Li et al., 2017). Skillful forecasting of severe thunderstorms requires knowledge of the environmental conditions that favor their occurrences.

Parameter-based climatologies of the environments associated with severe thunderstorms have been extensively studied. For example, in the United States, Rasmussen and Blanchard (1998) discriminated between the environments of non-supercell thunderstorms, supercells without significant tornadoes, and supercells with significant tornadoes using more than 6000 soundings. Hurlbut and Cohen (2014) investigated the environments of severe thunderstorms across the Northeastern United States and focused on distinguishing between the more prolific severe-weather-producing thunderstorms and those that produced only

isolated severe weather. In Europe, Groenemeijer and van Delden (2007) studied the sounding-derived parameters associated with large hail and tornadoes in the Netherlands. Taszarek and Kolendowicz (2013) documented the climatology of sounding-derived parameters associated with tornadoes in Poland. Tuovinen et al. (2015) examined the environmental characteristics of significant hailstorms in Finland using observed soundings. Kahraman et al. (2017) documented the environments of tornado and severe hail days in Turkey from 1979 to 2013 based on European Centre for Medium-Range Weather Forecasts (ECMWF) reanalysis data.

Hail growth has long been recognized as being favored in environments with properly high convective available potential energy (CAPE), as the strong updrafts in these environments are able to facilitate the suspension and subsequent growth of hailstones in the growth region (Nelson, 1983; Ziegler et al., 1983; Foote, 1984; Conway and Zrnić, 1993). The importance of vertical wind shear for hail formation has also been noted by a number of studies (Das, 1962; Berthet et al., 2013; Johnson and Sugden, 2014; Dennis and Kumjian, 2017). For example, Groenemeijer and van Delden (2007) found that the instability parameters and the 0–6 km vertical wind shear (SHR6) had considerable skill in distinguishing environments of large hail from those of non-hail-producing thunderstorms in the Netherlands. Púčik et al. (2015) showed that large hail typically occurred in high CAPE environments, with increased probability when conditions became more favorable for supercells (i.e., when CAPE and SHR6 increased). Taszarek et al. (2017) concluded that hail occurrence in Europe was generally greater with higher CAPE. For large hail, the SHR6 and boundary layer moisture were also important factors, apart from CAPE and steep temperature lapse rates. Li et al. (2018a) documented an eight-year climatology of hail events and their environments in China. Their results indicated that the hail diameter tended to increase with higher CAPE, larger SHR6, and higher precipitable water (PW). They further concluded that the environments for the largest hail with diameters greater than 30 mm were characterized by a median PW of 33.4 mm, a median CAPE of 2192 J kg^{-1}, and a median SHR6 of 21.5 m s^{-1}. In addition, a number of studies have documented that large hail is associated with a higher lifting condensation level (LCL, Rasmussen and Blanchard, 1998; Groenemeijer and van Delden, 2007; Grams et al., 2012; Púčik et al., 2015; Taszarek et al., 2017).

THWs can occur under a variety of CAPE and vertical wind shear environments (Evans and Doswell, 2001). While a great number of THWs are supported in high CAPE and strong vertical shear environments (Qin et al., 2006; Coniglio et al., 2010; Fan and Yu, 2013), many windstorms thrive in high shear, low CAPE environments (Evans and Doswell, 2001; Corfidi et al., 2006; Evans, 2010; Sherburn and Parker, 2014; Púčik et al., 2015). Numerous studies have discriminated between the THW environments and other convective environments. For example, Kuchera and Parker (2006) found that ground-relative wind velocity was most effective at discriminating between damaging and nondamaging wind environments in the United States. Parameters such as CAPE, humidity aloft, and lapse rates aloft were moderately discriminating. Liao (2009) studied the environments associated with THW events in Beijing and classified the events into dry and moist categories. Most dry THWs occurred in low CAPE and moderate-to-high shear environments, whereas the majority of the moist THWs were associated with moderate-to-high conditional instability. They also found that the downdraft CAPE, wind speeds in the middle and lower troposphere, and the lapse rate below the LCL, were useful indicators for the impending THWs. Taszarek et al. (2017) found that the THWs in Europe were most common in high shear and marginal CAPE conditions. The 0–3 km wind shear (SHR3) was the best parameter in distinguishing between severe and extremely severe THWs. Ma et al. (2019) demonstrated that thunderstorms producing extreme THWs in China were associated with drier middle troposphere, shallower low-level moist layer, significantly greater CAPE, and significantly higher SHR3 and SHR6 compared with ordinary thunderstorms.

Although SDHR is not categorized as one of the severe convective hazards in the United States, it is in China due to its high occurrence frequency and close association with flooding hazards (Chen et al., 2006; Jiang et al., 2014; Chen et al., 2016b; Zhang et al., 2018). The environments associated with SDHR have been widely studied in China and were found to differ markedly from those of hail and THWs (e.g., Hao et al., 2012; Tian et al., 2015; Chen et al., 2016b; Gao et al., 2018). For example, Fan and Yu (2013) concluded that the environments favorable to SDHR were characterized by lower mid-tropospheric lapse rates, higher dew-point temperature in the boundary layer, weaker vertical wind shear, and higher 0 °C, −20 °C, and equilibrium levels compared with hail and THWs. Tian et al. (2015) found that the PW discriminated the best between the environments of no precipitation, ordinary precipitation, and SDHR. Among various instability parameters, the best lifted index (LI) showed the greatest skill in distinguishing SDHR from the other two precipitation categories. The best CAPE and vertical wind shear were unable to discriminate between precipitation with different intensities.

The results of previous studies indicated that, although some characteristics were common to severe convection in different parts of the world, the magnitudes of the convective parameters varied from region to region, and the forecasting skill of these parameters for various weather types also exhibited regional differences. For example, it has been noted by a number of studies that the environmental CAPE in Europe is lower than that in the United States (Púčik et al., 2015; Tuovinen et al., 2015; Kahraman et al., 2017). Also, the LCL height has been proved to be a very useful parameter in tornado forecasting in the United States (Brooks and Craven, 2002; Craven et al., 2002; Thompson et al., 2003), but it shows limited skill in Europe where the LCL heights are generally lower (Groenemeijer and van Delden, 2007; Grünwald and Brooks, 2011; Taszarek and Kolendowicz, 2013; Taszarek et al., 2017). Further, the vertical wind shear associated with thunderstorms in China is generally lower than that in the United States (Meng et al., 2013; Fei et al., 2016). Therefore, it is important to study the local thunderstorm environments and determine which parameters show utility in discriminating between various weather phenomena in the region of interest.

The primary goal of the present study is to document the environmental conditions associated with different types of severe thunderstorms over North China using a set of environmental parameters. For the sake of comparison, the environments associated with non-severe thunderstorms and no-rain days were also examined. Each weather category was further grouped into mountain and plain classes to compare the environments over different altitudes. The remainder of this paper is organized as follows. Section 2 introduces data and methodology. Section 3 presents the results of single-parameter distributions associated with various categories through box-and-whisker plots. Section 4 examines the probability distributions of various categories in combined two-parameter spaces. A summary is given in Section 5.

2. Data and methodology

In this study, the 3-h severe weather reports (SWRs), 1-h precipitation observations, 1-h routine observations at surface weather stations, and the 0.25° × 0.25° 1-h ECMWF ERA5 reanalysis dataset (Copernicus Climate Change Service, 2017) during the warm seasons (May–September) of 2011–2018 over North China were used. The North China region was defined as the region covering 35°–45°N and 110°–125°E (Fig. 1). All observational data were obtained from the National Meteorological Center, China Meteorological Administration (CMA). According to the National Meteorological Center, severe convective weather refers to hail with diameters ≥ 5 mm, THWs with wind speeds ≥ Beaufort scale 8 or 17.2 m s^{-1}, SDHR with hourly precipitation ≥20 mm, and any tornado (Zheng et al., 2015). Tornadoes were not considered in this study. Therefore, thunderstorms that produced hail, THWs, or SDHR meeting the above criteria were deemed severe
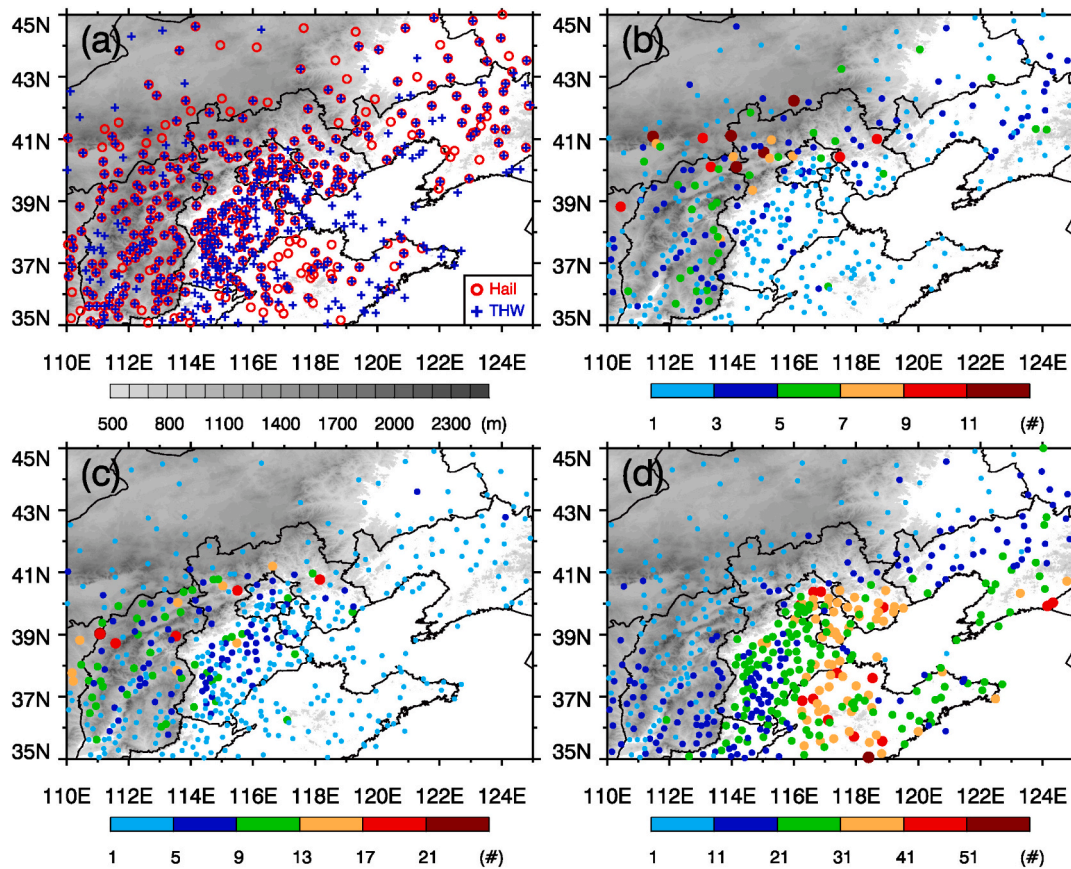
Fig. 1. Spatial distributions of (a) the 538 stations used for the determination of various categories in this study and the occurrence frequency of (b) hail, (c) THWs, and (d) SDHR during the study period based on the 538 stations. Red circles (plus signs) in (a) represent stations that have at least one occurrence of hail (THWs) during the study period. Gray shadings in all panels represent topography.

thunderstorms in this study.

2.1. The SWRs dataset

The SWRs dataset were used to obtain hail and THWreports. The dataset had a time interval of 3 h, giving eight files per day. In each file, all severe weather that occurred in the 3-h period were recorded with station ID, location (longitude and latitude), time (hour and minute), weather phenomena, and other information. Severe weather—including thunder, high winds, hail, tornadoes, snow, glaze, and those that caused obstruction to vision—were recorded if they met the criteria of the CMA. The wind speed and direction were provided for a high wind report, and the maximum diameter was provided for a hail report.

The high wind records in the SWRs included not only the convectively generated winds, but also a variety of nonconvective winds such as those related to cold air and those that are caused by topography. Since we were interested only in those caused by deep moist convection, the method described in Yang et al. (2017) was used to select THWs from all high wind reports. According to the regulations of the CMA, a new report was required if the wind speed reinforced or a mistake was found in a previous report. Therefore, there might be multiple reports within one SWR file for the same wind event. When this was the case, the latest report was retained and the previous one(s) were removed. This was also implemented for hail reports. After applying all these filters, a total of 467 and 365 stations in the SWRs dataset were retained, each of which had at least one occurrence of THWs and hail, respectively, during the study period and domain. It should be noted that underreporting of SWRs existed because these reports were based on point measurements, and those that did not occur at the observation stations were not reported. Also, the SWRs were unavoidably influenced by the spatial

inhomogeneity of the distribution of the stations. These problems are also present in the National Climatic Data Center's Storm Events Database, as have been noticed by a number of studies (Weiss and Bluestein, 2002; Gallus et al., 2008; Smith et al., 2012). In addition, the SDHR reports were obtained from the hourly surface precipitation observations.

2.2. Determination of different categories

The number of stations that conduct precipitation observation is much more than that conduct hail and THWs observations in the study area. To avoid great disparity in the sample size of various categories, we used a total of 538 stations that had at least one occurrence of hail or THWs for the determination of various categories in this study (i.e., the union of the 365 hail stations and 467 THW stations, Fig. 1a). The severe thunderstorm category was classified into four classes according to the convective hazards: only hail (H), only THW (W), only SDHR (R), and two or three types of the above three hazards (hybrid). To compare the environments favorable to severe thunderstorms with those associated with non-severe thunderstorms and no-rain days, two other weather categories—i.e., non-severe thunderstorms and no-rain—were included, which gave a total of six weather categories.

All hail, THW, and SDHR events were first retrieved using the dataset introduced above. Next, the four severe thunderstorm categories were determined based on the weather phenomenon in the 1-h window when the severe convective events occurred, owing to the fact that we assigned a severe convective event the most recent reanalysis sounding prior to the occurrence of the event (see the definition of proximity soundings in Section 2.3). For example, a hail report was recorded at a station at 1200–1300 Beijing Standard Time (BST, BST = UTC + 8 h). If

no other severe convective events (i.e., SDHR or THWs) were recorded at this station during this hour, then the sounding at 1200 BST in proximity to this station was deemed representative of the hail environments and was therefore labeled as an H sounding. If a THW report was recorded during 1200–1300 BST at this station, then the proximity sounding at 1200 BST was considered a hybrid one. A non-severe thunderstorm sample was determined when a thunder report was not accompanied by any of the severe convective weather (i.e., hail, THWs, and SDHR) in the SWRs dataset. To avoid the concurrence of severe and non-severe thunderstorms on the same day, non-severe thunderstorm samples were not included in the dataset if severe thunderstorms were observed over North China on that day. A no-rain sample was defined for a station if the 24-h precipitation was zero for all stations in a $4° \times 4°$ region centered at this station.

To avoid oversampling of the similar environments, all samples in the same weather category were required to be 6 h or 250 km away from each other in this study, as was done in Johnson and Sugden (2014). Similar but less stringent conditions were used in Thompson et al. (2003) and Reames (2017). Our study used more strict conditions to reduce the influence of duplicate samples on the statistical results as much as possible. The spatial distributions of the occurrence frequency of SDHR, hail, and THWs suggest that great variations exist regarding the frequency of these events between the mountainous and plain areas of North China (Fig. 1b–c). For example, the highest frequency for SDHR was found over the plains, whereas those for hail and THWs were observed over the mountains. In addition, previous studies have highlighted the differences in environmental conditions over the mountains and plains (Xiao et al., 2017; Yang and Sun, 2018). Therefore, each of the six weather categories in the present study was further divided into two groups—mountain and plain—to facilitate comparisons between the environments over different altitudes. A sample was labeled mountain (plain) if the station altitude was $\geq$ ($<$) 500 m.

2.3. Construction of proximity soundings

Due to their higher horizontal and temporal resolutions, reanalysis soundings have been used for climatological storm environment studies by a growing number of studies (Brooks et al., 2003, 2007; Markowski et al., 2003; Thompson et al., 2003, 2007; Allen and Karoly, 2014). However, some studies have highlighted the differences in the boundary layer variables between reanalysis and observed soundings and the necessity of correcting the boundary layer variables of the reanalysis soundings (Wang et al., 2012; Gensini et al., 2014; King and Kennedy, 2019). Therefore, the present study used a two-step procedure to create proximity soundings for all samples, which included creating reanalysis soundings using the ERA5 reanalysis dataset and correcting the low levels of the reanalysis soundings using 1-h surface observations.

Before the construction of proximity soundings, the spatial and temporal information of the ERA5 and surface observations have to be determined. In the present study, the time of both the reanalysis data and surface observations was determined as the closest hour prior to the sample for all weather categories except no-rain. In Schneider and Dean (2008) and Dean et al. (2009), severe weather reports were also mapped back to the most recent analysis prior to their occurrences. For no-rain samples, the time was set uniformly to 1400 BST to represent the environments with approximately the highest CAPE during the day. In the spatial sense, the reanalysis grid and the surface station were determined in different manners for the no-rain category and the rest of the categories. For no-rain samples, it was quite straightforward: the ERA5 grid closest to the sample station and the surface observations at this station were chosen. For samples associated with thunderstorms (i.e., all categories except for no-rain), we first determined an uncontaminated surface station closest to the sample. To do this, we started by identifying all surface stations in a $1° \times 1°$ box centered at the sample location whose precipitation amounts were zero in the preceding two hours (e.g., the precipitation during 1000–1200 BST needed to be zero for a 1230

BST sample). This was done by using the 1-h surface precipitation observations. Then, the nearest surface station to the sample location among all qualified stations was selected as the uncontaminated station. If no uncontaminated station was found for a sample, the sample was discarded. Second, the ERA5 grid closest to the uncontaminated station and the observations at the uncontaminated station were used to construct the proximity sounding for this sample.

The construction of the proximity soundings was as follows: first, a total of 32 isobaric layers (i.e., all layers from 1000 hPa to 10 hPa) of pressure, altitude, temperature, dew-point temperature, and horizontal wind at the identified ERA5 grid and time were subtracted. Next, observations at the identified surface station were used to correct the lower levels of ERA5 sounding (Johnson and Bresch, 1991; Pan et al., 2008; Fei et al., 2016; Yang and Sun, 2018). Specifically, if the interpolated surface temperature rising along the dry adiabatic line intersected with the temperature profile of the ERA5 sounding, the ERA5 temperature profile below the crossing layer was replaced with the dry adiabatic line rising from the surface temperature. If no intersection was found, then the surface data was deemed the lowest layer of the proximity sounding.

2.4. Computation of environmental parameters

After the proximity soundings were constructed, a variety of thermodynamic and wind shear parameters were calculated. These parameters were chosen based on the consideration of the key ingredients for severe thunderstorms: boundary layer moisture, conditional instability, a lifting mechanism that initiates convection, and vertical wind shear (Weisman and Klemp, 1982; Johns and Doswell, 1992). For the sake of brevity, a total of eight parameters were presented in the paper (Table 1): surface-based CAPE (SBCAPE), most unstable CAPE (MUCAPE), LI, SHR3, SHR6, LCL, PW, and pseudo-equivalent potential temperature at 500 hPa (thetase500). The virtual temperature correction was applied in the calculation of thermodynamic variables (Doswell and Rasmussen, 1994). The MUCAPE was calculated as the CAPE of the most buoyant parcel in the lowest 300 hPa (Doswell and Rasmussen, 1994). The LI was calculated as the temperature difference at 500 hPa between the environment and an air parcel that was lifted adiabatically from the surface to that level. The SHR3 (SHR6) was calculated as the magnitude of the vector difference between the 10-m wind and the wind at 3 km (6 km) above ground level (AGL). The PW was calculated by integrating the specific humidity from surface to 300 hPa.

A simple quality control was then performed for all severe and non-severe thunderstorm soundings based on the SBCAPE values. Specifically, non-severe thunderstorm soundings were removed if no SBCAPE was present, and severe thunderstorm soundings were removed if the SBCAPE was less than 50 J kg^{-1}. This was done to eliminate possibly nonrepresentative soundings. Similar restrictions were frequently used in storm environment studies (e.g., Brooks et al., 1994; Rasmussen and Blanchard, 1998; Craven et al., 2002; Tuovinen et al., 2015; Kahraman et al., 2017). After all these steps, the final dataset consisted of 391H soundings, 442 W soundings, 1585 R soundings, 318 hybrid soundings, 601 non-severe thunderstorm soundings, and 4188 no-rain soundings (Table 2).

The environmental parameters derived from corrected ERA5

Table 1
Parameters computed from proximity soundings in this study.

Parameter description	Abbreviation	Unit
Surface-based convective available potential energy	SBCAPE	J kg^{-1}
Most unstable convective available potential energy	MUCAPE	J kg^{-1}
Lifted index	LI	°C
0–3 km AGL bulk wind shear	SHR3	m s^{-1}
0–6 km AGL bulk wind shear	SHR6	m s^{-1}
Lifting condensation level	LCL	m AGL
Precipitable water from the surface to 300 hPa	PW	mm
Pseudo-equivalent potential temperature at 500 hPa	thetase500	K

Table 2
Numbers of proximity soundings for various categories.

	H	W	R	Hybrid	Non-severe thunderstorms	No-rain
Mountain	255	263	420	139	357	1921
Plain	136	179	1165	179	244	2267
Total	391	442	1585	318	601	4188

soundings were first evaluated against observational soundings (Appendix A). The results indicate that there is generally good agreement between the observational soundings and ERA5 soundings, which confirms the reliability of the results in the present study. Then, the box-and-whisker plots (Tukey, 1977) were applied to examine the single parameter distributions of various categories. As a rule of thumb, we considered two distributions significantly different when the upper or lower quartile of one box plot and the median of another showed no overlap (Tukey, 1977; Krzywinski and Altman, 2014; Reames, 2017). In addition, the probability distributions of various categories in paired parameter spaces were analyzed to determine the environments under which a certain type of weather was most likely to occur. All plots in the present study were generated using the Interactive Data Language (IDL) software (https://www.l3harrisgeospatial.com/Software-Technology/IDL).

3. Single parameter distributions

3.1. Instability

The instability parameters (SBCAPE, MUCAPE, and LI) are good discriminators between the environments supportive of severe thunderstorms (i.e., H, W, R, and hybrid), non-severe thunderstorms, and no-rain over both mountains and plains, except the fact that the SBCAPE and LI do not discriminate between non-severe thunderstorm and R environments over the plains (Figs. 2–4). This verifies the notion of atmospheric instability being one of the key ingredients for convective activity (Johns and Doswell, 1992). It is also suggested that the MUCAPE has better skill in discriminating between these categories than the SBCAPE, as the separation between these categories in the MUCAPE distribution is larger. It should be noted that, although the instability associated with the no-rain category is generally weak, a small proportion of the no-rain soundings have moderate-to-large CAPE values and large negative LI values, especially over the plains. This implies a potential false alarm issue in operational forecasting. The discriminating skill of the instability parameters between four severe thunderstorm categories is rather limited: the SBCAPE and MUCAPE do not discriminate between various severe thunderstorm categories, and the LI only discriminates between R and hybrid thunderstorms over the mountains

and plains and between H and R thunderstorms over the plains. Nevertheless, it is observed that the instabilities associated with the hybrid category are larger than those associated with the remaining three severe thunderstorm categories over both mountains and plains (except that the SBCAPE of the hybrid category is slightly lower than that of the H category over the plains), which indicates that the occurrence of two or more types of severe convective weather generally requires on average larger instability compared with when only one type of severe convective weather occurs. Among the H, W, and R categories, the greatest instabilities are observed in the H category, over both mountains and plains, indicating stronger instability associated with hail compared with THWs and SDHR. The fact that hail occurs in environments with higher CAPE than THWs was also reported in the Northeast United States (Hurlbut and Cohen, 2014) and Europe (Kaltenböck et al., 2009; Púčik et al., 2015; Taszarek et al., 2017).

Comparison between the distributions of mountain and plain groups demonstrates that all weather categories have stronger instabilities over the plains than over the mountains, with the exception of the SBCAPE for the hybrid category. The CAPE values for hail, THWs, and non-severe thunderstorms over North China are lower than those over the United States (SBCAPE for THWs, Klimowski et al., 2003; MUCAPE for hail, THWs, and non-severe thunderstorms, Kuchera and Parker, 2006; MUCAPE for hail, Johnson and Sugden, 2014), but higher than those in Europe (MUCAPE for hail and non-severe thunderstorms in the Netherlands, Groenemeijer and van Delden, 2007; MUCAPE for THWs in Finland, Punkka and Bister, 2015; MUCAPE for hail in Finland, Tuovinen et al., 2015; SBCAPE for hail in Turkey, Kahraman et al., 2017). It was also noted in Li et al. (2018a) that the CAPE associated with hail events in the European countries was generally smaller than in both the United States and China.

3.2. Vertical wind shear

Figs. 5 and 6 indicate that both the low-level and deep-layer shear have very limited skill in discriminating between various weather categories over North China. For SHR3, significant differences are only observed between H and no-rain categories and between H and R categories, over the mountains and plains. The SHR6 only distinguishes H from two other severe thunderstorm categories (i.e., W and R) over the plains, which indicates that hail occurrence over the plains requires significantly higher deep-layer shear than THWs and SDHR. Considerable overlap of the interquartile ranges is observed between the vertical wind shear distributions of the remaining categories. All categories save the R and no-rain have higher median vertical wind shear values over the plains than over the mountains. The deep-layer shear associated with hail and THWs over North China is notably lower than that over the United States (for THWs, Klimowski et al., 2003; for hail and THWs,
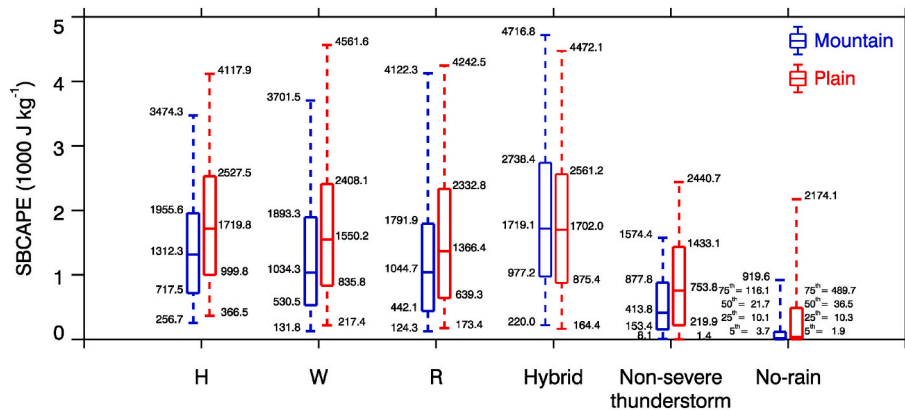

Fig. 2. Box-and-whisker plots of the SBCAPE (J kg^{-1}) associated with the six weather categories over the mountains (blue) and plains (red). The boxes denote the interquartile ranges. The horizontal lines inside the boxes denote the median values. The whiskers extend to the 5th and 95th percentiles.
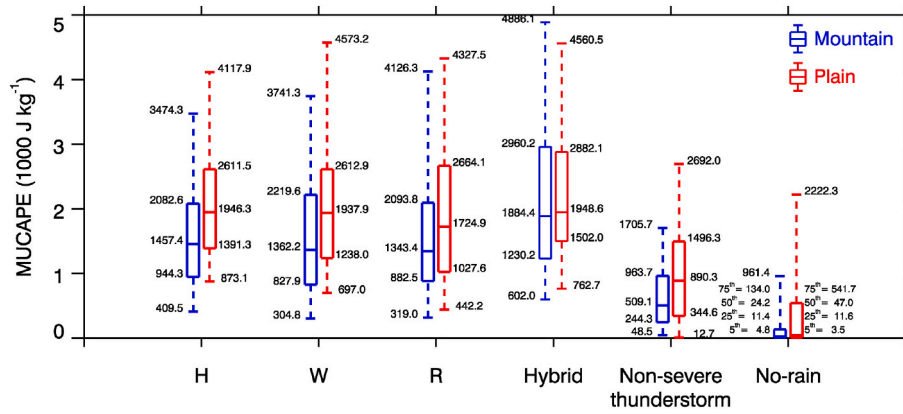
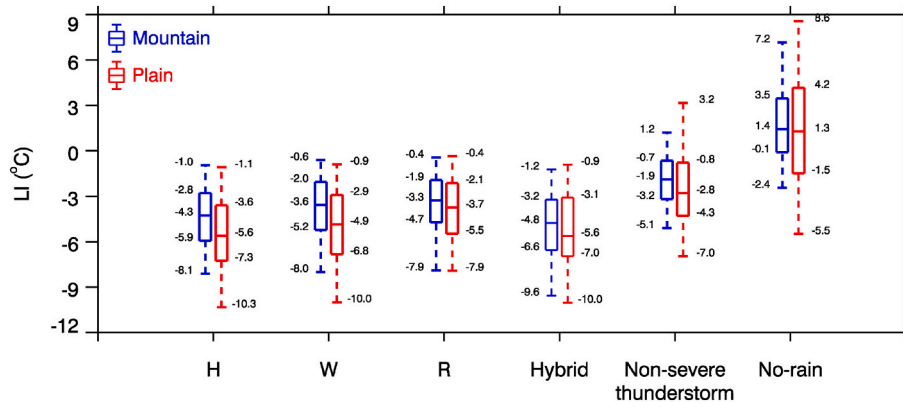**Fig. 3.** As in Fig. 2, but for MUCAPE (J kg^{-1}).
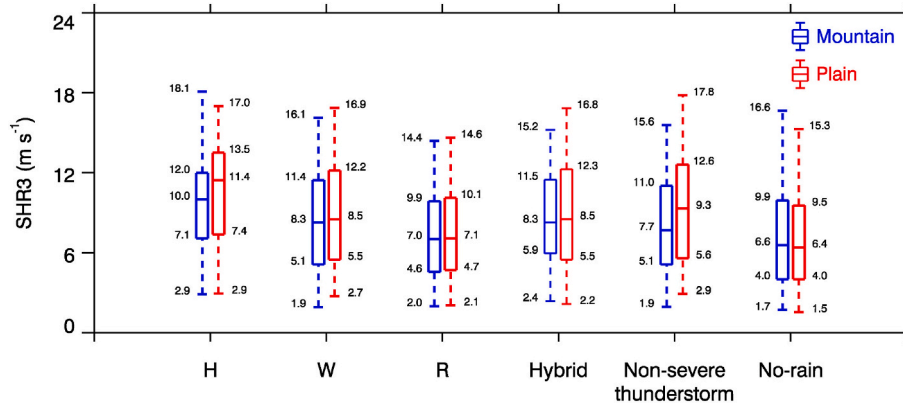

Fig. 4. As in Fig. 2, but for LI (°C).

Fig. 5. As in Fig. 2, but for SHR3 (m s^{-1}).

Kuchera and Parker, 2006; for hail, Johnson and Sugden, 2014), and the deep-layer shear for hail (THWs) over North China is comparable to (less than) that over Europe (for hail, Groenemeijer and van Delden, 2007; for hail and THWs, Púčik et al., 2015; for hail, Kahraman et al., 2017; for THWs, Taszarek et al., 2017). In addition, the deep-layer shear for non-severe thunderstorms over North China is larger than that over the United States (Rasmussen and Blanchard, 1998; Craven et al., 2002), and is comparable to that in the Netherlands (Groenemeijer and van Delden, 2007).

3.3. Moisture

The LCL heights of the no-rain category are significantly higher than those of the severe and non-severe thunderstorms (Fig. 7), and the LCL heights of the R are significantly lower than those of the remaining categories, over the mountains and plains. The LCL does not discriminate between H, W, and hybrid thunderstorms. It was also concluded in Brooks and Craven (2002) that LCL did not distinguish THWs environments from hail environments in the United States. Nevertheless, the LCL heights of the W are higher than those of the H over the mountains,
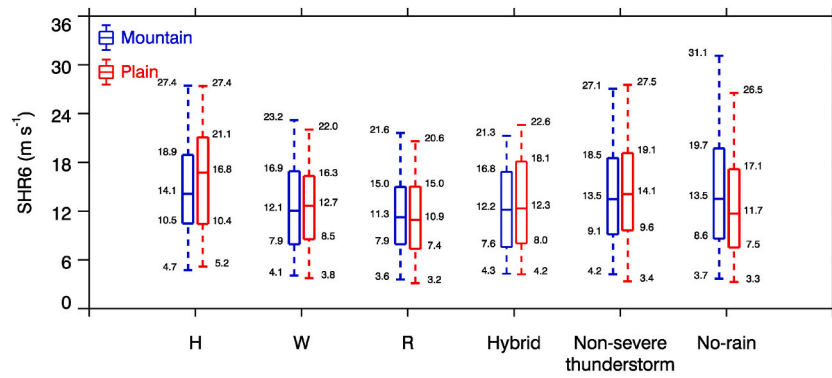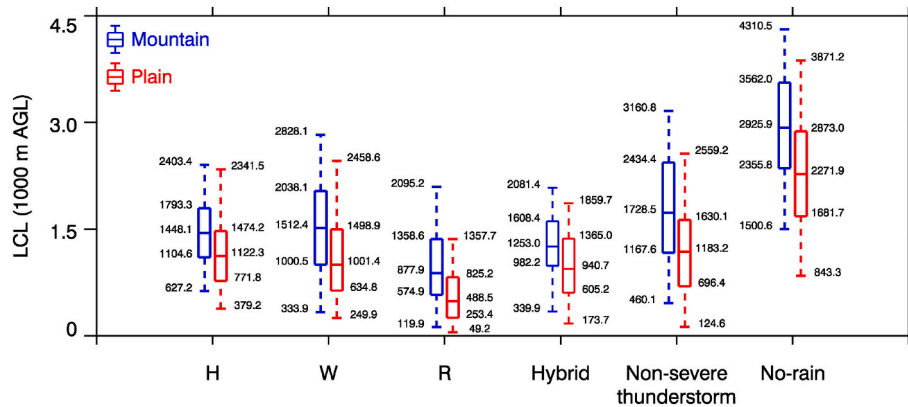
Fig. 6. As in Fig. 2, but for SHR6 (m s⁻¹).

Fig. 7. As in Fig. 2, but for LCL (m AGL).

whereas the contrary is true over the plains. This may be explained by the surface relative humidity associated with these two categories. An examination of the 2-m dew-point depression suggests that the surface is drier for W soundings over the mountains (the medians for H and W are 11.0 K and 12.0 K, respectively) and for H soundings over the plains (the medians for H and W are 9.0 K and 8.0 K, respectively). Over the United States (Kuchera and Parker, 2006) and central Europe (Púčik et al., 2015), it was found that hail was associated with higher LCL than THWs, which resembled the result over the North China plain. The LCL heights for all categories are lower over the plains than over the mountains, with the differences of all categories except H and hybrid being statistically significant.

As with the instability parameters, the PW shows considerable skill in discriminating between severe thunderstorm, non-severe

thunderstorm, and no-rain environments over both mountains and plains, except that the distributions of H and non-severe thunderstorms show minor overlap (Fig. 8). For mountain samples, 75% of the no-rain soundings have PW less than 15.4 mm, whereas less than 5% (25%) of the W (H) soundings are associated with these values, and a negligible fraction of the R and hybrid soundings are associated with these values. Therefore, a threshold of approximately 15 mm for PW can be used to discriminate between severe thunderstorms and no-rain days over the mountains. Likewise, a PW threshold of 25 mm can be used for such discrimination over the plains. The PW discriminates well between the R and two other severe thunderstorm categories (i.e., H and W), as well as between hybrid and H categories, over both mountains and plains. Over the plains, the PW also shows skill in discriminating between R and hybrid environments, as well as between H and W environments. These
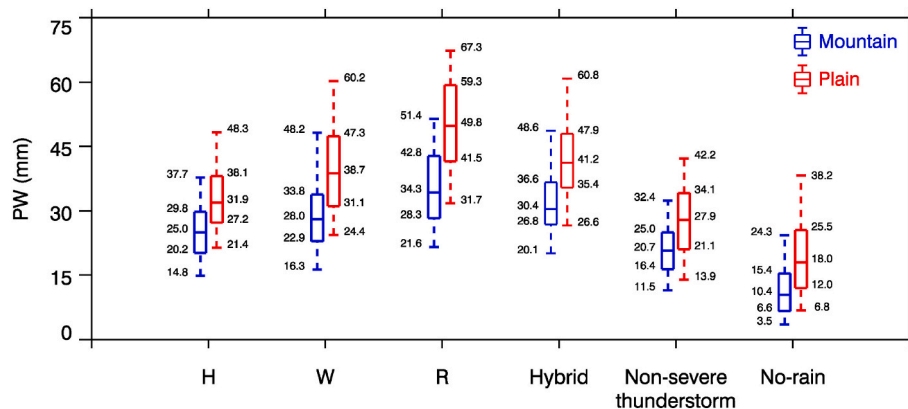

Fig. 8. As in Fig. 2, but for PW (mm).

results indicate that abundant moisture in the troposphere is crucial for the occurrence of SDHR. Despite not being statistically significant, the PW values for W are larger than those for H over the mountains. The PW values for all categories over the plains are significantly larger than those over the mountains, indicating more abundant water vapor over the plains. The PW values for THWs over North China are larger than those over the northern High Plains of the United States (Klimowski et al., 2003).

3.4. Mid-tropospheric environment

The thetase500 is used to represent the temperature and humidity conditions in the middle troposphere. The results indicate that the thetase500 is skillful in distinguishing no-rain environments from all severe thunderstorm environments over both mountains and plains, except that it does not discriminate between no-rain and H environments over the plains (Fig. 9). The thetase500 also discriminates between non-severe thunderstorms and all severe thunderstorm categories except H, over both mountains and plains. The thetase500 does not discriminate between non-severe thunderstorm and no-rain environments. One important finding about the thetase500 is that it discriminates between H and W environments over both mountains and plains, while no other parameters investigated in this study show such discriminatory skill (the PW only discriminates between these two categories over the plains). Indeed, previous studies (Fan and Yu, 2013; Gao et al., 2018) have shown that, although the distinction between SDHR environments and hail/THW environments can be achieved by some parameters, discrimination between H and W environments is difficult. Comparison of the thetase500 distributions between the mountains and plains shows that all categories except for R and no-rain have higher median thetase500 values over the mountains than over the plains.

4. Paired parameter distributions

The forecasting skill of individual parameters is often limited and better skill could be achieved through combinations of parameters (Davies and Johns, 1993; Johns et al., 1993). The combination of CAPE and SHR6 is frequently used in relevant studies (Brooks et al., 2003; Dean et al., 2009; Púčik et al., 2015; Taszarek et al., 2017) and is also inspected in this study. Since the PW shows the greatest skill in discriminating between various categories on the whole, and the thetase500 is the only parameter that discriminates between H and W soundings over both mountains and plains, we also examined the probability of occurrence frequency associated with various categories in the PW–thetase500 space. The parameter values associated with the maximum probability of occurrence in these paired parameter spaces are given in Table 3.

Table 3
Parameter values associated with the box(s) with the maximum probability in the MUCAPE–SHR6 space (Fig. 10) and PW–thetase500 space (Fig. 11).

		MUCAPE–SHR6	PW–thetase500
H	Mountain	[~1300 J kg^{-1}, ~17.5 m s^{-1}]	[~21 mm, ~324 K]
	Plain	[~1500 J kg^{-1}, ~20.5 m s^{-1}] [~1700 J kg^{-1}, ~16.5 m s^{-1}]	[~31 mm, ~322 K]
W	Mountain	[~900 J kg^{-1}, ~11.5 m s^{-1}] [~500 J kg^{-1}, ~14.5 m s^{-1}] [~1100 J kg^{-1}, ~15.5 m s^{-1}]	[~26 mm, ~328 K]
	Plain	[~1500 J kg^{-1}, ~11.5 m s^{-1}]	[~31 mm, ~322 K]
R	Mountain	[~900 J kg^{-1}, ~11.5 m s^{-1}]	[~26 mm, ~327 K] [~32 mm, ~331 K] [~37 mm, ~336 K]
	Plain	[~1700 J kg^{-1}, ~9.5 m s^{-1}]	[~43 mm, ~330 K]
Hybrid	Mountain	[~2700 J kg^{-1}, ~17.5 m s^{-1}]	[~27 mm, ~326 K]
	Plain	[~900 J kg^{-1}, ~19.5 m s^{-1}] [~1700 J kg^{-1}, ~9.5 m s^{-1}] [~1800 J kg^{-1}, ~19.5 m s^{-1}] [~2900 J kg^{-1}, ~12.5 m s^{-1}]	[~35 mm, ~326 K]
Non-severe thunderstorm	Mountain	[~500 J kg^{-1}, ~12.5 m s^{-1}]	[~23 mm, ~326 K]
	Plain	[~100 J kg^{-1}, ~21.5 m s^{-1}]	[~33 mm, ~322 K]
No-rain	Mountain	[~100 J kg^{-1}, ~10.5 m s^{-1}]	[~9 mm, ~318 K]
	Plain	[~100 J kg^{-1}, ~9.5 m s^{-1}]	[~11 mm, ~316 K]

4.1. MUCAPE–SHR6 space

A shift of the high occurrence probability toward larger MUCAPE values in the MUCAPE–SHR6 space is evident from the no-rain to the non-severe thunderstorm and to the severe thunderstorm category, over both mountains and plains (Fig. 10). The no-rain soundings are mostly likely to be associated with small MUCAPE values (< 200 J kg^{-1}) over both mountains and plains. However, large MUCAPE values do appear in the no-rain category, especially over the plains, as noted earlier (Figs. 2 and 3).
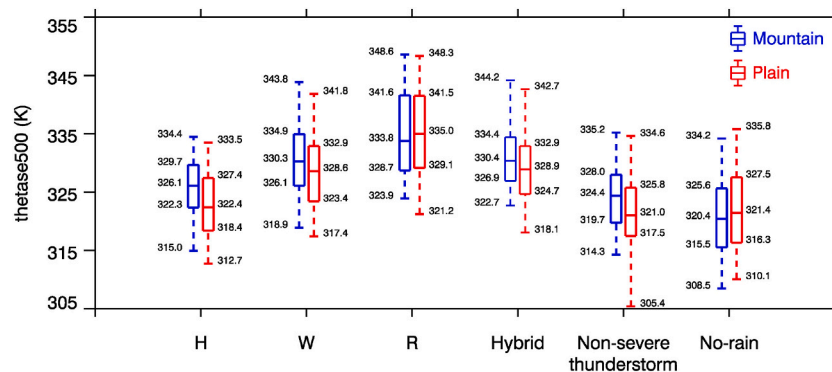

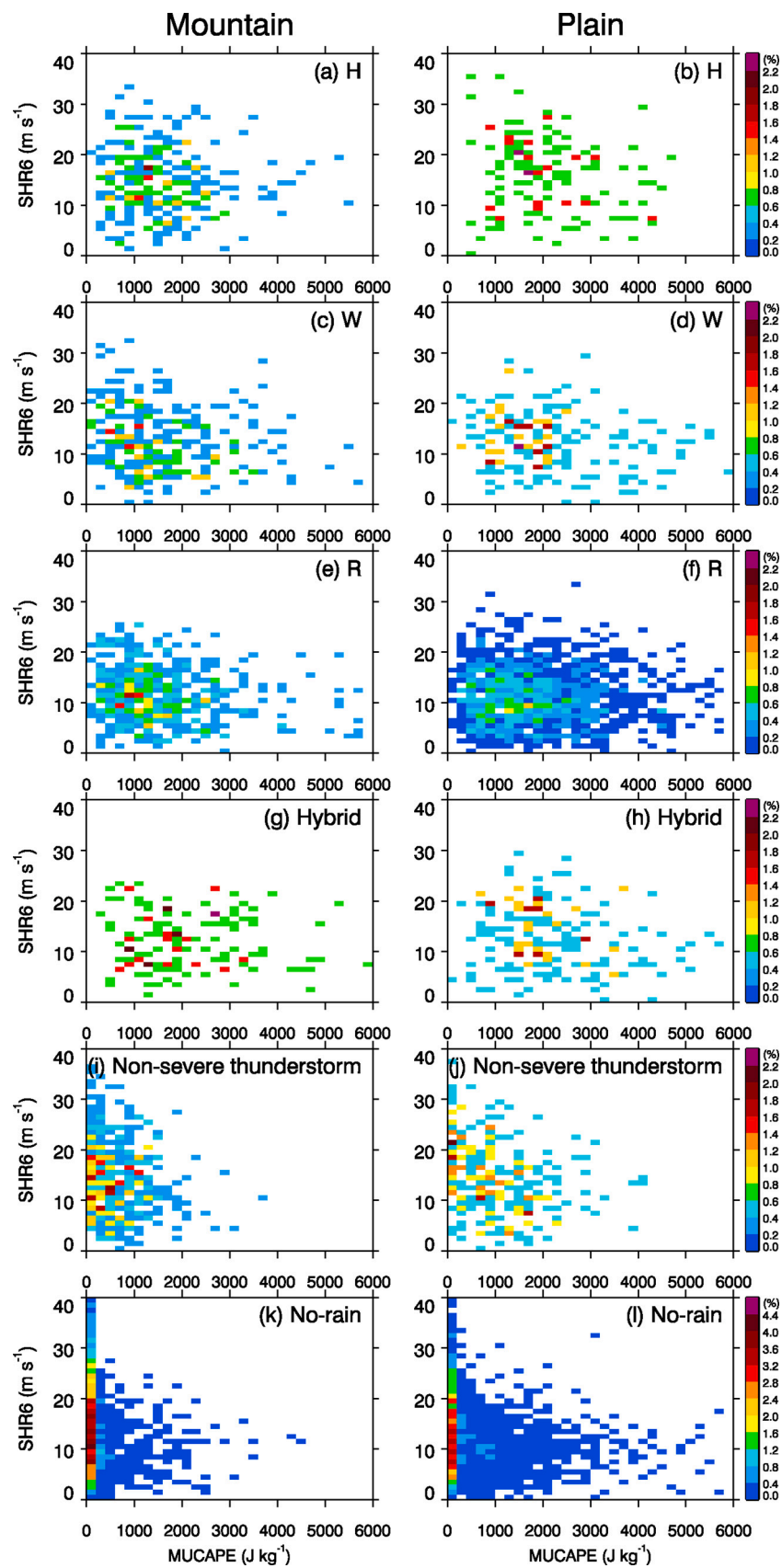**Fig. 9.** As in Fig. 2, but for thetase500 (K).

Fig. 10. Probability distributions of the occurrence frequency of (a, b) H, (c, d) W, (e, f) R, (g, h) hybrid, (i, j) non-severe thunderstorm, and (*k,l*) no-rain categories over mountains (left) and plains (right) in the MUCAPE–SHR6 space. Note that the color bar scale for the no-rain category (k, l) differs from the others (a–j).

Over the mountains, the majority of the H and W soundings are located in the similar MUCAPE regime (i.e., 400–2800 J kg^{-1}), but the MUCAPE associated with the maximum probability of H ($\sim$1300 J kg^{-1}) is larger than that of W (400–1200 J kg^{-1}). As for SHR6, 64% of the H soundings are observed in moderate and high deep-layer shear environments (i.e., SHR6 > 12 m s^{-1}; Johns and Doswell, 1992) with the maximum probability appearing at 17.5 m s^{-1}, whereas a smaller fraction (52%) of the W soundings are associated with modetate-to-high deep-layer shear environments. The occurrence frequency of W is maximized in three MUCAPE–SHR6 regimes: low MUCAPE ($\sim$900 J kg^{-1}) and weak SHR6 ($\sim$11.5 m s^{-1}), low MUCAPE ($\sim$500 J kg^{-1}) and moderate SHR6 ($\sim$14.5 m s^{-1}), and moderate MUCAPE ($\sim$1100 J kg^{-1}) and moderate SHR6 ($\sim$15.5 m s^{-1}). These results indicate that H is more frequently associated with larger instability and higher deep-layer shear compared with W. The distribution of R is concentrated in a regime of 200–1800 J kg^{-1} MUCAPE and 5–17 m s^{-1} SHR6 with the maximum probability appearing at MUCAPE of $\sim$900 J kg^{-1} and SHR6 of $\sim$11.5 m s^{-1}. The lower SHR6 of R compared with H and W suggests that the occurrence of R depends less on the deep-layer shear than H and W. The distribution of the hybrid category shows more dependence on the instability, as the majority of the samples are located in the moderate and high MUCAPE regime while spanning a wide range of SHR6 values. The maximum probability is observed in a remarkably higher MUCAPE ($\sim$2700 J kg^{-1}, which is more than twice of that for H) and a larger SHR6 ($\sim$17.5 m s^{-1}, which is comparable to that of H) regime, compared with H, W, and R. This indicates that the severe thunderstorms producing hybrid severe convective weather over the mountains are most likely to occur in environments with the highest instability and the strongest deep-layer shear.

Over the plains, H tends to occur in moderate-to-high MUCAPE environments (only a small fraction of the H soundings are observed in the <1000 J kg^{-1} MUCAPE space), which confirms that modest MUCAPE is necessary for the occurrence of H over the plains. Note that while some of the H soundings are observed in the low SHR6 regime (i.e., around 10 m s^{-1}), a great number of the soundings are concentrated in the moderate-to-high SHR6 regime (i.e., 16–28 m s^{-1}). The highest probability of H is observed in a regime of 1400–1800 J kg^{-1} MUCAPE and 16–21 m s^{-1} SHR6. The majority of the W soundings are located in a similar MUCAPE but notably lower SHR6 regime compared with H. The maximum probability of W is found in a moderate MUCAPE ($\sim$1500 J kg^{-1}) and marginally moderate deep-layer shear ($\sim$11.5 m s^{-1}) environment. The distribution of the R category is characterized by more occurrences in the small MUCAPE regime (< 1000 J kg^{-1}) compared with other severe thunderstorm categories, with the maximum probability locating in MUCAPE of $\sim$1700 J kg^{-1} and SHR6 of $\sim$9.5 m s^{-1}. The highest probability of the hybrid category is rather dispersedly distributed, spanning from low ($\sim$900 J kg^{-1}) to high ($\sim$2900 J kg^{-1}) MUCAPE and from weak ($\sim$9.5 m s^{-1}) to strong ($\sim$21.5 m s^{-1}) SHR6.

4.2. PW–thetase500 space

Fig. 11 shows that the distributions of the no-rain category in the PW–thetase500 space differ significantly from those of the severe thunderstorm categories over both mountains and plains, as large probabilities of the no-rain category are confined in the PW < 20 mm and thetase500 < 325 K space, while those of the severe thunderstorms are basically located in the remaining regime. In a similar way, but with smaller degrees of separation in the parameter space, the distributions of non-severe thunderstorms also differ from those of severe thunderstorms.

Over the mountains, many of the H soundings are concentrated in a regime of 18–32 mm PW and 321–331 K thetase500, with the maximum appearing at PW of $\sim$21 mm and thetase500 of $\sim$324 K. For W, the probability distribution extends toward space with larger PW and larger thetase500 values compared with H, especially in the thetase500 dimension. This indicates that hail tends to occur in environments with

drier and cooler mid-troposphere compared with THWs. A shift toward larger PW values is found in the distribution of R when compared with those of W and H. While a number of H and W soundings (particularly H) are found in the <20 mm PW space, negligible R soundings are observed in such environments. The distribution of the hybrid category is densely clustered in a regime of 26–34 mm PW and 323–333 K thetase500. Similar to R, hybrid-type severe thunderstorms rarely occur in environments with PW < 20 mm. Over the plains, R is most commonly favored in environments with the highest PW (38–54 mm) and the highest thetase500 (325–335 K) among four types of severe thunderstorm categories, followed by hybrid (PW of 34–46 mm and thetase500 of 323–333 K) and W (PW of 30–44 mm and thetase500 of 321–333 K). H is concentrated in a regime with the lowest PW (24–34 mm) and the lowest thetase500 (315–325 K) among all severe thunderstorm categories.

Comparisons of the mountain and plain groups reveal that the distributions of all six weather categories displaced markedly toward higher PW values during the progression from mountain to plain. The H and W categories are also more likely to occur in higher thetase500 environments over the mountains than over the plains, whereas the distributions of the remaining categories show little displacement in the thetase500 dimension from mountain to plain.

5. Summary and conclusions

Using proximity soundings taken during the warm seasons of 2011–2018 over North China, this work analyzed the environments associated with severe thunderstorms, non-severe thunderstorms and no-rain days. The severe thunderstorm category was further broken down into four classes based on the convective hazards: H, W, R, and hybrid. In total, 391H soundings, 442 W soundings, 1585 R soundings, 318 hybrid soundings, 601 non-severe thunderstorm soundings, and 4188 no-rain soundings were obtained. Soundings in each weather category were further classified into mountain and plain groups to facilitate comparisons of the environmental conditions at different altitudes. A set of parameters was evaluated for their skill in discriminating various weather categories over both mountains and plains.

Generally, stronger instability, more abundant moisture, and higher vertical wind shear are present over the plains than over the mountains, although only the differences associated with PW are significant for all weather categories. Over both mountains and plains, the instability parameters (SBCAPE, MUCAPE, and LI) are good discriminators between the environments supportive of severe thunderstorms (i.e., H, W, R, and hybrid), non-severe thunderstorms, and no-rain, but are rather limited in discriminating between the environments associated with four types of severe thunderstorms; the vertical wind shear parameters show very limited skill in discriminating between various weather categories; the LCL is useful in distinguishing no-rain and R environments from those of other categories; the PW shows the greatest skill for the discrimination of various weather categories; and the thetase500 is the only parameter investigated in this study that discriminates between H and W environments. The discrimination skill of these parameters over mountains and plains are generally the same, although disagreements do exist. For example, the PW does not distinguish R from hybrid severe thunderstorms over the mountains whereas it does over the plains.

Probability distributions in the MUCAPE–SHR6 space show that a shift of the high probability region toward larger MUCAPE values in the MUCAPE–SHR6 space is evident from the no-rain to the non-severe thunderstorm and to the severe thunderstorm category, over both mountains and plains. Over the mountains, the occurrence probability of the hybrid category is maximized in environments with the largest MUCAPE and the highest SHR6 among all severe thunderstorms; H is most likely to occur in moderate MUCAPE and moderate SHR6 environments, R is most likely to occur in marginally moderate MUCAPE and marginally moderate SHR6 environments, and the occurrence of W is favored in different MUCAPE–SHR6 environments. Over the plains, the
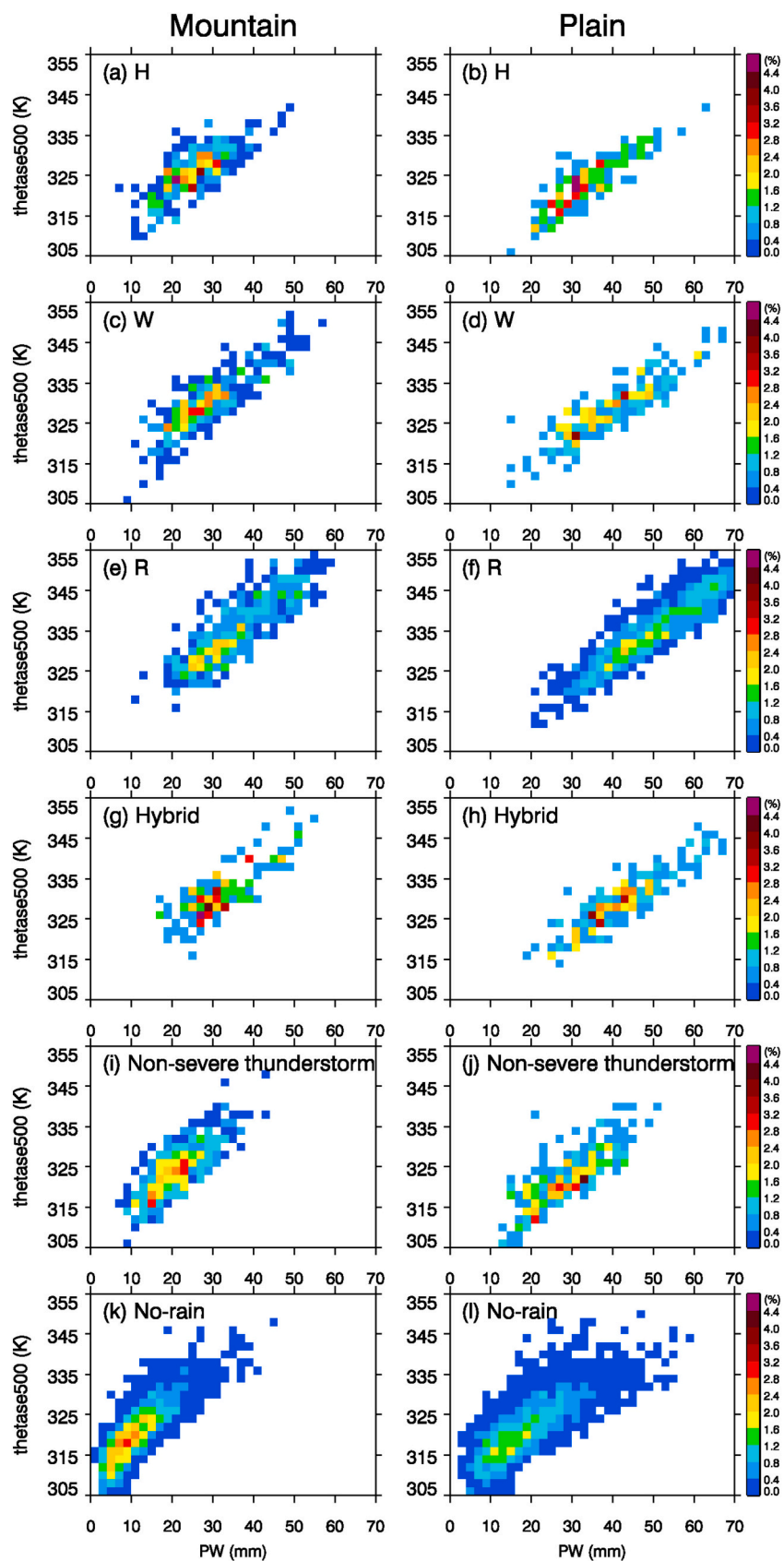
Fig. 11. As in Fig. 10, but for the distributions in the PW–thetase500 space. The color bars are the same for all panels.

majority of the H, W, and hybrid thunderstorms occur in moderate and high MUCAPE environments; the H occurrence shows great dependence on large deep-layer shear, while W and R probilities are maximized in marginally moderate and weak deep-layer shear environments, respectively; the hybrid category are frequently favored in both weak and moderate SHR6 environments. Probability distributions in the PW–thetase500 space show that there is considerable separation between the distributions of severe thunderstorms and those of no-rain and those of non-severe thunderstorms. Over both mountains and plains, high probabilities of R is displaced toward higher PW and thetase500 space compared with the remaining three severe thunderstorm categories, especially over the plains; H tends to occur in environments with the lowest PW and thetase500 among different types of severe thunderstorms.

It is without doubt that further studies are needed to gain deeper insight into the severe thunderstorm environments over this region. For example, the high-shear and low-CAPE environments present a unique challenge in operations and more research on the convection characteristics in these environments is needed. In addition, composite parameters with enhanced forecasting ability need to be developed based on the skill of individual parameters, which can better guide the severe thunderstorm forecasting in this region.

Declaration of Competing Interest

The authors declare that they have no known competing financial interests or personal relationships that could have appeared to influence the work reported in this paper.

Acknowledgements

Appendix A. Supplementary data

Supplementary data to this article can be found online at https://doi.org/10.1016/j.atmosres.2021.105519.

References

Allen, J.T., Karoly, D.J., 2014. A climatology of Australian severe thunderstorm environments 1979–2011: Inter-annual variability and ENSO influence. Int. J. Climatol. 34, 81–97. https://doi.org/10.1002/joc.3667.

Berthet, C., Wesolek, E., Dessens, J., Sanchez, J.L., 2013. Extreme hail day climatology in Southwestern France. Atmos. Res. 123, 139–150. https://doi.org/10.1016/j.atmosres.2012.10.007.

Brooks, H.E., Craven, J.P., 2002. A database proximity soundings for significant severe thunderstorms, 1957–1993. In: Preprints, 21th Conference on Severe Local Storms, San Antonio, TX, Amer. Meteor. Soc, pp. 639–642.

Brooks, H.E., Doswell, C.A., Cooper, J., 1994. On the environments of tornadic and nontornadic mesocyclones. Weather Forecast. 9, 606–618. https://doi.org/10.1175/1520-0434(1994)009<0606:OTEOTA>2.0.CO;2.

Brooks, H.E., Lee, J.W., Craven, J.P., 2003. The spatial distribution of severe thunderstorm and tornado environments from global reanalysis data. Atmos. Res. 67–68, 73–94. https://doi.org/10.1016/S0169-8095(03)00045-0.

Brooks, H.E., Anderson, A.R., Riemann, K., Ebbers, I., Flachs, H., 2007. Climatological aspects of convective parameters from the NCAR/NCEP reanalysis. Atmos. Res. 83, 294–305. https://doi.org/10.1016/j.atmosres.2005.08.005.

Chen, M.X., Yu, X.D., Tan, X.G., Gao, F., 2006. Radar echoes characteristics of the sudden convective rainstorm over Beijing area on July 10, 2004. J. Appl. Meteor. Sci. 17, 333–345. CNKI:SUN:YYQX.0.2006-03-011 (in Chinese).

Chen, M.X., Wang, Y.C., Gao, F., Xiao, X., 2012. Diurnal variations in convective storm activity over contiguous North China during the warm season based on radar mosaic climatology. J. Geophys. Res. 117, D20115 https://doi.org/10.1029/2012JD018158.

Chen, J., Zheng, Y.G., Zhang, X.L., Zheng, P.J., 2013. Distribution and diurnal variation of warm-season short-duration heavy rainfall in relation to the MCSs in China. Acta Meteor. Sinica. 27, 868–888. https://doi.org/10.1007/s13351-013-0605-x.

Chen, M.X., Xiao, X., Gao, F., Lei, L., Wang, Y.C., Sun, J.Z., 2016a. A case study and batch verification on high resolution numerical simulations of severe convective events using an analysis based on rapid-refresh 4-D variational radar data assimilation. Acta Meteorologica Sinica. 74, 421–441. https://doi.org/10.11676/qxxb2016.031 (in Chinese).

Chen, Y.Z., Yu, X.D., Chen, X.L., 2016b. Characteristics of short-time severe rainfall events based on weather flow and key environmental parameters in Pearl River Delta. Meteor. Mon. 42, 144–155. https://doi.org/10.7519/j.issn.1000-0526.2016.02.002 (in Chinese).

Coniglio, M.C., Hwang, J.Y., Stensrud, D.J., 2010. Environmental factors in the upscale growth and longevity of MCSs derived from rapid update cycle analyses. Mon. Wea. Rev. 138, 3514–3539. https://doi.org/10.1175/2010MWR3233.1.

Conway, J.W., Zrnić, D.S., 1993. A study of embryo production and hail growth using dual-Doppler and multiparameter radars. Mon. Wea. Rev. 121, 2511–2528. https://doi.org/10.1175/1520-0493(1993)121<2511:ASOEPA>2.0.CO;2.

Copernicus Climate Change Service (C3S), 2017. ERA5: Fifth generation of ECMWF atmospheric reanalyses of the global climate. In: Copernicus Climate Change Service Climate Data Store (CDS) accessed 22nd November 2019. https://cds.climate.copernicus.eu/cdsapp#!/home.

Corfidi, S.F., Corfidi, S.J., Imy, D.A., Logan, A.L., 2006. A preliminary study of severe wind-producing MCSs in environments of limited moisture. Weather Forecast. 21, 715–734. https://doi.org/10.1175/WAF947.1.

Craven, J.P., Brooks, H.E., Hart, J.A., 2002. Baseline climatology of sounding derived parameters associated with deep, moist convection. Preprints. In: 21st Conference on Severe Local Storms, San Antonio, TX, Amer. Meteor. Soc, pp. 643–646.

Das, P., 1962. Influence of wind shear on the growth of hail. J. Atmos. Sci. 19, 407–414. https://doi.org/10.1175/1520-0469(1962)019<0407:IOWSOT>2.0.CO;2.

Davies, J.M., Johns, R.H., 1993. Some wind and instability parameters associated with strong and violent tornadoes. 1: Wind shear and helicity. In: The Tornado: Its Structure, Dynamics, Prediction, and Hazards, Geophys. Monogr, 79. Amer. Geophys. Union, pp. 573–582.

Dean, A.R., Schneider, R.S., Thompson, R.L., Hart, J., Bothwell, P.D., 2009. The conditional risk of severe convection estimated from archived NWS/storm Prediction Center mesoscale objective analyses: potential uses in support of forecast operations and verification. In: 23rd Conf. on Weather Analysis and forecasting/19th Conf. On Numerical Weather Prediction. Amer. Meteor. Soc, Omaha, NE, 6A.5. https://ams.confex.com/ams/pdfpapers/154304.pdf.

Dennis, E.J., Kumjian, M.R., 2017. The impact of vertical wind shear on hail growth in simulated supercells. J. Atmos. Sci. 74, 641–663. https://doi.org/10.1175/JAS-D-16-0066.1.

Doswell, C.A., Rasmussen, E.N., 1994. The effect of neglecting the virtual temperature correction on CAPE calculations. Weather Forecast. 9, 625–629. https://doi.org/10.1175/1520-0434(1994)009<0625:teontv>2.0.co;2.

Evans, M., 2010. An examination of low CAPE/high shear severe convective events in the Binghamton, New York county warning area. Natl. Wea. Dig. 34, 129–144.

Evans, J.S., Doswell, C.A., 2001. Examination of derecho environments using proximity soundings. Weather Forecast. 16, 329–342. https://doi.org/10.1175/1520-0434(2001)016<0329:EODEUP>2.0.CO;2.

Fan, L.M., Yu, X.D., 2013. Characteristic analyses on environmental parameters in short-term severe convective weather in China. Plateau Meteor. 32, 156–165. https://doi.org/10.7522/j.issn.1000-0534.2012.00016 (in Chinese).

Fei, H.Y., Wang, X.M., Zhou, X.G., 2016. Climatic characteristics and environmental parameters of severe thunderstorm gales in China. Meteor. Mon. 42, 1513–1521. https://doi.org/10.7522/j.issn.1000-0534.2016.00083 (in Chinese).

Foote, G.B., 1984. A study of hail growth utilizing observed storm conditions. J. Climate Appl. Meteor. 23, 84–101. https://doi.org/10.1175/1520-0450(1984)023<0084:ASOHGU>2.0.CO;2.

Gallus, W.A., Snook, N.A., Johnson, E.V., 2008. Spring and summer severe weather reports over the Midwest as a function of convective mode: a preliminary study. Weather Forecast. 23, 101–113. https://doi.org/10.1175/2007WAF2006120.1.

Gao, X.M., Yu, X.D., Wang, L.J., Wang, W.B., Wang, S.J., Wang, X.H., Han, X., 2018. Characteristics of environmental parameters for classified severe convective weather in central area of Shandong province. Acta Meteor. Sinica. 76, 196–212. https://doi.org/10.11676/qxxb2018.006 (in Chinese).

Gensini, V.A., Mote, T.L., Brooks, H.E., 2014. Severe-thunderstorm reanalysis environments and collocated radiosonde observations. J. Appl. Meteor. Climatol. 53, 742–751. https://doi.org/10.1175/JAMC-D-13-0263.1.

Grams, J.S., Thompson, R.L., Snively, D.V., Prentice, J.A., Hodges, G.M., Reames, L.J., 2012. A climatology and comparison of parameters for significant tornado events in the United States. Weather Forecast. 27, 106–123. https://doi.org/10.1175/WAF-D-11-00008.1.

Groenemeijer, P.H., van Delden, A., 2007. Sounding-derived parameters associated with large hail and tornadoes in the Netherlands. Atmos. Res. 83, 473–487. https://doi.org/10.1016/j.atmosres.2005.08.006.

Grünwald, S., Brooks, H.E., 2011. Relationship between sounding derived parameters and the strength of tornadoes in Europe and the USA from reanalysis data. Atmos. Res. 100, 479–488. https://doi.org/10.1016/j.atmosres.2010.11.011.

Hao, Y., Yao, Y.Q., Zheng, Y.Y., Lu, J., 2012. Multi-scale analysis and nowcasting of short-time heavy rainfall. Meteor. Mon. 38, 903–912. CNKI:SUN:QXXX.0.2012-08-004 (in Chinese).

Hurlbut, M.M., Cohen, A.E., 2014. Environments of Northeast U.S. severe thunderstorm events from 1999 to 2009. Weather Forecast. 29, 3–22. https://doi.org/10.1175/WAF-D-12-00042.1.

Jiang, X.M., Yuan, H.L., Xue, M., Chen, X., Tan, X.G., 2014. Analysis of a heavy rainfall event over Beijing during 21–22 July 2012 based on high resolution model analyses and forecasts. J. Meteor. Res. 28, 199–212. https://doi.org/10.1007/s13351-014-3139-y.

Johns, R.H., Doswell, C.A.I.I.I., 1992. Severe local storms forecasting. Weather Forecast. 7, 588–612. https://doi.org/10.1175/1520-0434(1992)007,0588:SLSF.2.0.CO;2.

Johns, R.H., Davies, J.M., Leftwich, P.M., 1993. Some wind and instability parameters associated with strong and violent tornadoes. In: Part II: Variations in the Combinations of Wind and Instability Parameters. The Tornado: Its Structure, Dynamics, Hazards, and Prediction, Geophys. Monogr, 79. Amer. Geophys. Union, pp. 583–590. https://doi.org/10.1029/GM079p0583.

Johnson, R.H., Bresch, J.F., 1991. Diagnosed characteristics of precipitation systems over Taiwan during the May June 1987 TAMEX. Mon. Wea. Rev. 119, 2540–2557. https://doi.org/10.1175/1520-0493(1991)119<2540:DCOPSO>2.0.CO;2.

Johnson, A.W., Sugden, K.E., 2014. Evaluation of sounding-derived thermodynamic and wind-related parameters associated with large hail events. Electronic J. Severe Storms Meteor. 9, 1–42 [Available online at http://www.ejssm.org/ojs/index.php/ejssm/article/viewArticle/137.].

Kahraman, A., Kadioglu, M., Markowski, P.M., 2017. Severe convective storm environments in Turkey. Mon. Wea. Rev. 145, 4711–4725. https://doi.org/10.1175/MWR-D-16-0338.1.

Kaltenböck, R., Diendorfer, G., Dotzek, N., 2009. Evaluation of thunderstorm indices from ECMWF analyses, lightning data and severe storm reports. Atmos. Res. 93, 381–396. https://doi.org/10.1016/j.atmosres.2008.11.005.

King, A.T., Kennedy, A.D., 2019. North American supercell environments in atmospheric reanalysis and RUC-2. J. Appl. Meteor. Climatol. 58, 71–92. https://doi.org/10.1175/JAMC-D-18-0015.1.

Klimowski, B.A., Bunkers, M.J., Hjelmfelt, M.R., Covert, J.N., 2003. Severe convective windstorms over the northern high plains of the United States. Weather Forecast. 18, 502–519. https://doi.org/10.1175/1520-0434(2003)18<502:SCWOTN>2.0.CO;2.

Krzywinski, M., Altman, N., 2014. Points of significance: Visualizing samples with box plots. Nat. Methods 11, 119–120. https://doi.org/10.1038/nmeth.2813.

Kuchera, E.L., Parker, M.D., 2006. Severe convective wind environments. Weather Forecast. 21, 595–612. https://doi.org/10.1175/WAF931.1.

Li, H.Q., Cui, X.P., Zhang, D.-L., 2017. On the initiation of an isolated heavy-rain-producing storm near the central urban area of the Beijing metropolitan region. Mon. Wea. Rev. 145, 181–197. https://doi.org/10.1175/MWR-D-16-0115.1.

Li, M.X., Zhang, D.-L., Sun, J.S., Zhang, Q.H., 2018a. A statistical analysis of hail events and their environmental conditions in China during 2008–15. J. Appl. Meteor. Climatol. 57, 2817–2833. https://doi.org/10.1175/JAMC-D-18-0109.1.

Li, X.F., Zhang, Q.H., Zou, T., Lin, J.P., Kong, H., Ren, Z.H., 2018b. Climatology of hail frequency and size in China, 1980-2015. J. Appl. Meteor. Climatol. 57, 875–887. https://doi.org/10.1175/JAMC-D-17-0208.1.

Liao, X.N., 2009. Analysis on environmental condition for wind gust in Beijing area. Climatic Environ. Res. 14, 54–62. https://doi.org/10.3878/j.issn.1006-9585.2009.01.06 (in Chinese).

Ma, S.P., Wang, X.M., Yu, X.D., 2019. Environmental parameter characteristics of severe wind with extreme thunderstorm. J. Appl. Meteor. Sci. 30, 292–301. CNKI:SUN: YYQX.0.2019-03-004 (in Chinese).

Markowski, P.M., Hannon, C., Frame, J., Lancaster, E., Pietrycha, A., Edwards, R., Thompson, R.L., 2003. Characteristics of vertical wind profiles near supercells obtained from the Rapid Update Cycle. Weather Forecast. 18, 1262–1272. https://doi.org/10.1175/1520-0434(2003)018,1262:COVWPN.2.0.CO;2.

Meng, Z.Y., Yan, D.C., Zhang, Y.J., 2013. General features of squall Lines in East China. Mon. Wea. Rev. 141, 1629–1647. https://doi.org/10.1175/MWR-D-12-00208.1.

Nelson, S.P., 1983. The influence of storm flow structure on hail growth. J. Atmos. Sci. 40, 1965–1983. https://doi.org/10.1175/1520-0469(1983)040<1965:TIOSFS>2.0.CO;2.

Pan, Y.J., Zhao, K., Pan, Y.N., 2008. Single-Doppler radar observation of a heavy-precipitation supercell on a severe squall line. Acta Meteor. Sinica. 66, 621–636. CNKI:SUN:QXXB.0.2008-04-014 (in Chinese).

Púčik, T., Groenemeijer, P., Rýva, D., Kolár, M., 2015. Proximity soundings of severe and non-severe thunderstorms in Central Europe. Mon. Wea. Rev. 143, 4805–4821. https://doi.org/10.1175/MWR-D-15-0104.1.

Punkka, A.-J., Bister, M., 2015. Mesoscale convective systems and their synoptic-scale environment in Finland. Weather Forecast. 30, 182–196. https://doi.org/10.1175/WAF-D-13-00146.1.

Qin, L., Li, Y.D., Gao, S.T., 2006. The synoptic and climatic characteristic studies of thunderstorm winds in Beijing. Climatic Environ. Res. 11, 754–762. https://doi.org/10.3969/j.issn.1006-9585.2006.06.010 (in Chinese).

Rasmussen, E.N., Blanchard, D.O., 1998. A baseline climatology of sounding-derived supercell and tornado forecast parameters. Weather Forecast. 13, 1148–1164. https://doi.org/10.1175/1520-0434(1998)013,1148:ABCOSD.2.0.CO;2.

Reames, L.J., 2017. Diurnal variations in severe weather forecast parameters of Rapid Update Cycle-2 tornado proximity environments. Weather Forecast. 32, 743–761. https://doi.org/10.1175/WAF-D-16-0029.1.

Schneider, R.S., Dean, A.R., 2008. A comprehensive 5-year severe storm environment climatology for the continental United States. In: 24th Conf. On Severe Local Storms. Amer. Meteor. Soc, Savannah, GA, 16A.4.

Sherburn, K.D., Parker, M.D., 2014. Climatology and ingredients of significant severe convection in high-shear, low-CAPE environments. Weather Forecast. 29, 854–877. https://doi.org/10.1175/WAF-D-13-00041.1.

Smith, B.T., Thompson, R.L., Grams, J.S., Broyles, C., Brooks, H.E., 2012. Convective modes for significant severe thunderstorms in the contiguous United States. Part I: Storm classification and climatology. Weather Forecast. 27, 1114–1135. https://doi.org/10.1175/WAF-D-11-00115.1.

Sun, J.S., Yang, B., 2008. Meso-β scale torrential rain affected by topography and the urban circulation. Chinese J. Atmos. Sci. 32, 1352–1364. https://doi.org/10.3878/j.issn.1006-9895.2008.06.10 (in Chinese).

Sun, J.H., Zhao, S.X., Fu, S.M., Wang, H.J., Zheng, L.L., 2013. Multi-scale characteristics of record heavy rainfall over Beijing area on July 21, 2012. Chinese J. Atmos. Sci. 37, 705–718. https://doi.org/10.3878/j.issn.1006-9895.2013.12202 (in Chinese).

Taszarek, M., Kolendowicz, L., 2013. Sounding-derived parameters associated with tornado occurrence in Poland and universal tornadic index. Atmos. Res. 134, 186–197. https://doi.org/10.1016/j.atmosres.2013.07.016.

Taszarek, M., Brooks, H.E., Czernecki, B., 2017. Sounding-derived parameters associated with convective hazards in Europe. Mon. Wea. Rev. 145, 1511–1528. https://doi.org/10.1175/MWR-D-16-0384.1.

Thompson, R.L., Edwards, R., Hart, J.A., Elmore, K.L., Markowski, P., 2003. Close proximity soundings within supercell environments obtained from the Rapid Update Cycle. Weather Forecast. 18, 1243–1261. https://doi.org/10.1175/1520-0434(2003)018,1243:CPSWSE.2.0.CO;2.

Thompson, R.L., Mead, C.M., Edwards, R., 2007. Effective storm-relative helicity and bulk shear in supercell thunderstorm environments. Weather Forecast. 22, 102–115. https://doi.org/10.1175/WAF969.1.

Tian, F.Y., Zheng, Y.G., Zhang, T., Zhang, X.L., Mao, D.Y., Sun, J.H., Zhao, S.X., 2015. Statistical characteristics of environmental parameters for warm season short-duration heavy rainfall over central and eastern China. J. Meteor. Res. 29, 370–384. https://doi.org/10.1007/s13351-014-4119-y.

Tukey, J.W., 1977. Exploratory Data Analysis. Addison Wesley, Reading, MA.

Tuovinen, J., Rauhala, J., Schultz, D.M., 2015. Significant-hail-producing storms in Finland: Convective-storm environment and mode. Weather Forecast. 30, 1064–1076. https://doi.org/10.1175/WAF-D-14-00159.1.

Wang, X.M., Yu, X.D., Zhu, H., 2012. The applicability of NCEP reanalysis data to severe convection environment analysis. J. Appl. Meter. Sci. 23, 139–146. https://doi.org/10.7519/j.issn.1000-0526.2011.4.004 (in Chinese).

Weisman, M.L., Klemp, J.B., 1982. The dependence of numerically simulated convective storms on vertical wind shear and buoyancy. Mon. Wea. Rev. 110, 504–520. https://doi.org/10.1175/1520-0493(1982)110,0504:TDONSC.2.0.CO;2.

Weiss, C.C., Bluestein, H.B., 2002. Airborne pseudo-dual doppler analysis of a dryline-outflow boundary intersection. Mon. Wea. Rev. 130, 1207–1226. https://doi.org/10.1175/1520-0493(2002)130<1207:APDDAO>2.0.CO;2.

Xiao, X., Sun, J.Z., Chen, M.X., Qie, X.S., Wang, Y.C., Ying, Z.M., 2017. The characteristics of weakly forced mountain-to-plain precipitation systems based on radar observations and high-resolution reanalysis. J. Geophys. Res. Atmos. 122, 3193–3213. https://doi.org/10.1002/2016JD025914.

Yang, X.L., Sun, J.H., 2018. Organizational modes of severe wind-producing convective systems over North China. Adv. Atmos. Sci. 35, 540–549. https://doi.org/10.1007/s00376-017-7114-2.

Yang, X.L., Sun, J.H., Zheng, Y.G., 2017. A 5-yr climatology of severe convective wind events over China. Weather Forecast. 32, 1289–1299. https://doi.org/10.1175/WAF-D-16-0101.1.

Zhang, X.W., Zheng, Y.G., Sheng, J., Cao, Y.C., 2018. Application and verification of extreme forecast index in severe convection weather. J. Meteor. Sci. 38, 768–779. https://doi.org/10.3969/2017jms.0088 (in Chinese).

Zheng, Y.G., Zhou, K.H., Sheng, J., Lin, Y.J., Tian, F.Y., Tang, W.Y., Lan, Y., Zhu, W.J., 2015. Advances in techniques of monitoring, forecasting and warning of severe convective weather. J. Appl. Meteor. Sci. 26, 641–657. https://doi.org/10.11898/1001-7313.20150601 (in Chinese).

Ziegler, C.L., Ray, P.S., Knight, N.C., 1983. Hail growth in an Oklahoma multicell storm. J. Atmos. Sci. 40, 1768–1791. https://doi.org/10.1175/1520-0469(1983)040<1768:HGIAOM>2.0.CO;2.